Development of a current sensor based on active materials for high-voltage transmission systems

2006 Smart Mater. Struct. 15 563

(http://iopscience.iop.org/0964-1726/15/2/039)

INSTITUTE OF PHYSICS PUBLISHING SMART MATERIALS AND STRUCTURES
Smart Mater. Struct. **15** (2006) 563–570 doi:10.1088/0964-1726/15/2/039

Development of a current sensor based on active materials for high-voltage transmission systems

Oscar Lopez-Garcia[1], **Alberto Carnicero, Rosa Ruíz, Juan Antonio Talavera and Carlos Mateo**

Instituto de Investigación Tecnológica, Universidad Pontificia Comillas de Madrid, Santa Cruz de Marcenado, 26, 28015 Madrid, Spain

E-mail: oscar.lopez@upcomillas.es

Received 16 May 2005, in final form 9 January 2006
Published 23 February 2006
Online at stacks.iop.org/SMS/15/563

Abstract
This paper presents the development of a new class of current sensor based on active materials for high-voltage transmission systems. This current sensor is an innovative design with respect to conventional current measurement transformers. The alternating current signal to be measured induces a magnetic field in an emitter which consists of a magnetostrictive material. The emitter transforms the current magnetic energy into mechanical energy in the form of mechanical waves due to the alternating nature of the induced magnetic field. These waves are transmitted through a dielectric structure until a piezoelectric stack, the receiver, is reached which converts the mechanical energy back into electrical energy. An electronic signal module processes this low electrical current and estimates the primary current to be measured. A numerical model has been developed to evaluate the preliminary design. A small scale prototype has been built and tested to demonstrate the feasibility of the current sensor. Experimental data have been used to fit the damping parameters of the model.

(Some figures in this article are in colour only in the electronic version)

1. Introduction

Instrument transformers are devices for voltage and electrical current measurements, which are key elements within modern transmission and distribution systems. These devices provide the basic input signals required for controlling the power flows in any electrical grid. Their importance has grown even higher in nowadays complex power networks due to the tighter and precise control required within a sector undergoing profound changes due to European, and worldwide, electrical market deregulation. Conventional transformers for measurement of elevated electrical currents in high-voltage grids have secondary windings to produce proportionally reduced electrical currents, i.e. 5 or 1 A, which are suitable for measurement. For lines with voltage levels of more than 220 kV, such instruments usually support currents higher than 2000 A, and these inductive measurement transformers become large, heavy and expensive devices. So, as the power of the electrical networks is steadily increasing worldwide, manufacturers of instrument transformers and electrical utility companies are becoming ever more concerned with this problem.

Many research studies have been developed and technical proposals have appeared looking for the resolution of this issue. Fibre optic technology has attracted the attention of the high-voltage community because it is based on dielectric materials, such as plastic or silicon dioxide fibres, that are able to transport signals. Fibre optic measurement transformers can be classified into two major categories: passive and active fibre optic approaches [13]. The former is probably the most conventional and it uses the fibre optic as a simple carrier of the signals of the sensors from the high-voltage side to the processing circuits of the secondary side. The

[1] Author to whom any correspondence should be addressed.

latter uses the fibre optic as an active measurement element itself; either the measurement is generated in the fibre itself or an optical device which is optically coupled to the fibre is used; see for instance [14, 16]. The major drawbacks of the fibre optic alternatives are the several factors that affect the measurements, such as temperature, vibrations and linearity [1, 8], as well as others related to the complexity of the required electronic circuits and cost of the system. In fact, several prototypes using fibre optics to measure electrical current have been built and tested in real power transmission lines but none has reached a stage of wide commercial acceptance.

In contrast, other technological fields have started the development of new concepts based on hybrid smart structures. For instance, magnetostrictive and piezoelectric composites have been developed for high-voltage miniature transformer applications [7], a hybrid Tonpilz transducer based on a magnetostrictive tube and piezoelectric ring stack driver was studied in [2], magnetic field sensors have been developed using magnetostrictive–piezoelectric materials [17], piezoelectric sensors and shape memory alloys washers have been applied to self-repairing bolted joint design [15], and a smart wing using a shape memory alloy tube as torsion actuator and piezoelectric ultrasonic motors in the trailing edge control surface has been studied in [19].

In this paper a measurement transformer based on active materials for high-voltage transmission lines is presented. This new approach is based on mechanical wave transmission due to coupling between active materials through a dielectric medium. This feature constitutes the main difference from the aforementioned hybrid smart structures. From the electrical point of view, the dielectric medium is responsible for dropping the voltage down to low voltage in order to protect the measurement parts of the transformer. If the performance of the current sensor takes into consideration not only the input/output ratio but also safe operation in high-voltage applications, the addition of a dielectric medium improves the global performance. This sort of transformer reduces the weight, volume, manufacturing cost and avoids the necessity of isolating oil, when compared to traditional measurement transformers that use magnetic flux variations. Regarding fibre optic approaches, this current sensor features lower complexity and lower cost electronic circuits and provides more thermal stable behaviour. Despite the evident improvements, depending on the sort of active material used, active material sensors can exhibit more or less performance ageing. Other difficulties derived from the use of active material can arise, such as hysteretic behaviour or intrinsic nonlinear behaviour.

The goal of this paper is to show the feasibility of this new class of measurement transformer. In order to demonstrate the validity of the design, the development of a small prototype have been carried out as a prior step to manufacturing a full-size device. To help the design process a numerical simulation program has been established. The requirements of such a program have been simplicity, robustness and low computational cost. Therefore, the numerical simulation program is based on simple active material constitutive modelling, i.e. one-dimensional and weak coupling between fields. Another objective of this paper is to show that the functioning principle works as expected by means of direct comparison between measurements and numerical simulations. Despite the simplicity of the numerical models used in the prototype design the results obtained are able to reproduce the experimental response quite closely.

The remainder of the paper is organized as follows. Section 2 summarizes the basic functioning of the proposed current sensor. Section 3 provides a brief description of the numerical modelling used to evaluate the current sensor design. Section 4 outlines the experimental program to evaluate the performance of the current sensor and shows the comparison between numerical simulation and experimental data. Finally, in section 5 the main conclusions of this study are drawn.

2. Description of the current sensor

The current sensor is made of two main parts: the active structure and auxiliary structure. Figure 1(a) shows a sketch of the active structure together with the auxiliary structure. The active structure which is located inside auxiliary structure is essentially formed by an emitter element (E), a dielectric medium (D) and a receiver (R). The emitter (E) is based on a magnetostrictive material that generates longitudinal elastic waves due to the alternating magnetic field induced by the primary current to be measured (I). Thus, the magnetic energy induced in the magnetostrictive emitter is converted into mechanical energy in the form of longitudinal elastic waves that propagate through a dielectric coupling structure until the receiver is reached. The dielectric medium (D) is used not only to propagate longitudinal elastic waves but also to electrically isolate both the receiver and the electronic signal processing module from the high voltage of the electrical line. Evidently, as the length of the dielectric medium increases so do the energy losses. However, this length is determined by the voltage drop required by the receiver to operate, from the electrical point of view, in safe conditions. Basically, the receiver (R) is made of a stack of piezoelectric discs. The receiver transforms the mechanical energy transmitted by the longitudinal elastic waves into electrical energy in the form of a low alternating electrical signal. Finally, these electrical signals are then filtered, amplified, and processed through the electronic signal processing module (ESPM) in order to obtain a measurement of the high primary current. The ESPM estimates the primary current from the piezoelectric output signal using an inverse function of the results of the fitted numerical model and experimental data.

In order to obtain a measurable electrical signal at the receiver, the auxiliary structure provides sufficient stiffness to the active structure; see figures 1(a) and 2(a) for further details. Broadly speaking, this auxiliary structure is made of a compression device (C), and top (T) and body (B) structures. The compression device (C) is basically a screw which applies the precompression level to the active structure. The top structure (T) provides the housing for the primary current cable (I) and compression device (C). The body structure (B) is a hollow cylinder of alumina. Both top and body structures are mechanical parts used to couple all the elements together and provide sufficient stiffness to consider the mechanical structure as if it was almost clamped. The body structure not only contributes to the global stiffness of the auxiliary structure but

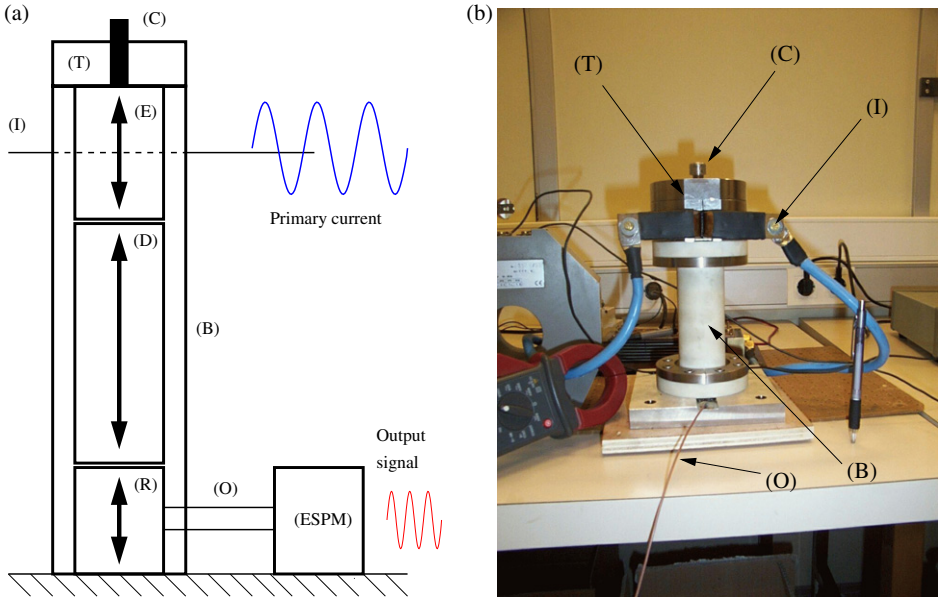

Figure 1. Proposed current sensor: (a) functioning diagram and (b) small-scale sensor.

Table 1. Main dimensions of the small-scale current sensor.

Component	Material	Length ($\times 10^{-3}$ m)	Diameter ($\times 10^{-3}$ m)
Emitter	TXRE	20	20
Dielectric	Alumina	160	20
Receiver	PZT5 Type II	4	20
Compression	Stainless steel	35	20
Top	Stainless steel	60	Inner 25, outer 100
Body	Alumina	155	Inner 25, outer 50

also enhances the electrical isolation. Due to these reasons, alumina was selected as the material for the body structure. In figure 1(b) the actual small-scale current sensor is shown. Basically, only the auxiliary structure can be seen in this figure. The body cylindrical structure, labelled as (B), together with compression device (C) and top structure (T) encapsulates the primary current cable (I). The output signal of the receiver is connected to the electronic signal processing module by the cable at the bottom (O). Despite the fact that high-current-carrying cables can usually vibrate a lot, the mechanical design of the auxiliary structure provides sufficient stiffness to isolate this vibration from the active structure which is responsible for the measurement of the output signal.

The current sensor shown in figures 1 and 2 corresponds to a small-scale current sensor and has been built to demonstrate the feasibility of the principle of functioning presented herein in order to be developed for high-voltage applications. The dimensions of each part of the small-scale sensor are several times lower than the actual current sensor. The dimensions of the small-scale sensor are listed in table 1. In order to reproduce normal operation, the magnetostrictive emitter must be used under high-current conditions while the level of voltage is not so relevant. Due to current sensor size and power limitation reasons, the small-scale sensor has been tested under high-current and low-voltage conditions.

The design process has implied the development of a virtual prototype and its finite element model in order to evaluate, prior to the manufacturing of the current sensor, the performance of the system. The active structure has been modelled by means of the finite element method and the auxiliary mechanical structure has been taken into account using lumped techniques. An exploded view of the current sensor is depicted in figure 2(a), and figure 2(b) sketches the structural model used in the simulation of the proposed current measurement transformer. The structural model consists of a continuous longitudinal structure made of magnetostrictive, dielectric and piezoelectric materials, denoted by subscripts m, d and p respectively. The auxiliary structure corresponds to lumped mass, denoted by m, and stiffness, k, contributions of compression, top and body structures, denoted by subscripts c, t and b respectively. Both active and auxiliary structures are mechanically coupled through the displacement of the top structure, u_t.

3. Active sensor modelling

The active sensor modelling stage was developed to evaluate that the virtual design of the current sensor was able to fulfil the initial requirements needed by the measurement transformer. The most relevant requirements for such a sensor are a minimum level of electrical output signal that could be measured and processed by the electronic signal processing module and stable response in a frequency range of the current transmission line as well as maximum signal to noise ratio.

To model the dynamic performance of the current sensor one-dimensional modelling has been chosen. One-dimensional models are worth considering in order to obtain both accurate and computational low-cost solutions. The one-dimensional structural model is based on the assumption

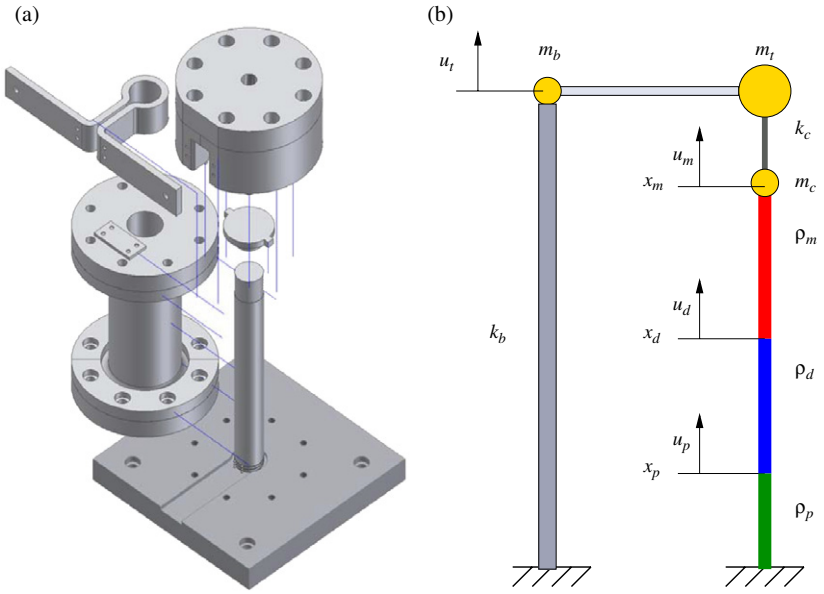

Figure 2. Small-scale current sensor: (a) exploded view and (b) structural model.

that only longitudinal modes are responsible for mechanical wave propagation along the active structure of the current measurement transformer. This assumption relies not only on physical considerations but also on published results elsewhere showing that this assumption provides sufficient accuracy to properly describe the actual response of similar devices; see for instance [5]. Thus, longitudinal displacement of the structure will be considered as the fundamental degree of freedom to model the dynamics of the current measurement transformer. The active sensor modelling stage has been mainly concerned with operational parameters that describe the performance of the current measurement transformer and the goal was to provide the foundation to develop and manufacture the current sensor.

Considering the active sensor model shown in figure 2(b), the axial linear momentum balance equation reads as

$$\begin{aligned} \frac{\partial T_{\mathrm{m}}}{\partial x} &= \rho_{\mathrm{m}} \frac{\partial^2 u_{\mathrm{m}}}{\partial t^2} \\ \frac{\partial T_{\mathrm{d}}}{\partial x} &= \rho_{\mathrm{d}} \frac{\partial^2 u_{\mathrm{d}}}{\partial t^2} \\ \frac{\partial T_{\mathrm{p}}}{\partial x} &= \rho_{\mathrm{p}} \frac{\partial^2 u_{\mathrm{p}}}{\partial t^2} \end{aligned} \tag{1}$$

where $u(x, t)$ is the axial displacement field, $T(x, t)$ the stress field, ρ the density, and x and t are position and time variables. Constitutive equations are required to formally well pose the problem of finding the dynamic response of the current sensor. In what follows, the constitutive models are introduced.

3.1. Magnetostriction model

One of the main approaches followed in magnetostrictive modelling is based on the thermodynamic mean field theory of Jiles and Atherton; see for instance [3, 6, 10–12, 18]. Despite the fact that this model describes the hysteretic behaviour of magnetostriction, one important drawback that it exhibits is the difficulty to obtain standard model parameters for magnetostrictive materials, and experiments must be conducted to obtain them. Nonlinear coupled constitutive relationships based on Gibbs free energy are developed in [4]. This model couples thermal and mechanical fields which can result in high computational cost models, specially in finite element implementations. Finally, one ingredient of the aforementioned models is the phenomenological relationship between magnetic field and magnetostrictive strain. This sort of model fails to take into account magnetostrictive irreversible behaviour. However, as it will be seen latter, it is accurate enough to provide a good description of induced strain by magnetostriction and it is quite easy to obtain reliable material properties.

Table 2. Properties of magnetostrictive material (TXRE).

Parameter	Symbol	Units	$T_0 = 3$ MPa	$T_0 = 7$ MPa
Density	ρ	kg m^{-3}	9200	9200
Elastic compliance	s^H	m^2 N^{-1}	3.3×10^{-11}	2.8×10^{-11}
Constant	a_2	m^2 A^{-2}	1.4×10^{-12}	4.1×10^{-12}

The magnetostrictive model adopted in this paper corresponds to the phenomenological behaviour between magnetostrictive and magnetic field as follows:

$$S_{\mathrm{m}} = s^H (T_{\mathrm{m}} - T_0) + \lambda_{\mathrm{m}}$$

where S_{m} is the magnetostrictive strain, s^H the elastic compliance at constant magnetic field, T_0 is the precompression stress, and λ_{m} is the magnetostrictive induced strain. From a phenomenological point of view this induced strain can be expressed by

$$\lambda_{\mathrm{m}} = a_2(T_0) H^2(x, t)$$

in which a_2 is a magnetostrictive constant and H is the magnetic field. The advantage of such a model is that it

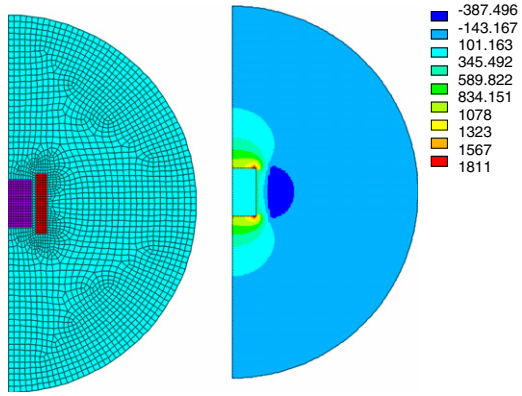

Figure 3. (a) Axisymmetric finite element mesh of the emitter plus air, (b) vertical component of the magnetic field on the emitter.

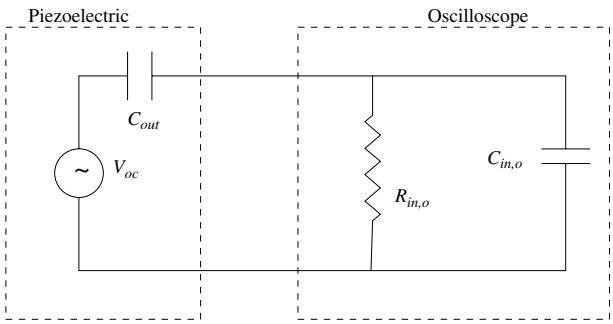

Figure 4. Equivalent electronic circuit scheme of the open circuit test.

provides accurate enough results with low computational cost. The properties of the magnetostrictive material used in the simulations are shown in table 2.

The contribution of the induced magnetostrictive strain has been added as a force. Therefore, the coupling between magnetic and mechanical fields is neglected. This weak coupling assumption is quite reasonable and has been used elsewhere; see for instance [3, 6].

Hence, to determine the magnetostrictive strain the magnetic field H must be computed. An axisymmetric electromagnetic finite element model has been used to determine the magnetic field created by the primary current on the magnetostrictive emitter. In figure 3(a) the mesh of the axisymmetric model is shown. The mesh consists of three main parts: the inner rectangular part is the magnetostrictive material, the outer rectangular part is the current conductor, and the main semicircle the air. In figure 3(b) the vertical component of the magnetic field is presented. Once the magnetic field distribution is computed the induced magnetostrictive strain field can be obtained.

3.2. Dielectric model

The dielectric material can be modelled as a linear elastic material. Therefore the constitutive equation is

$$S_\mathrm{d} = s_\mathrm{d} T_\mathrm{d}$$

Table 3. Properties of dielectric material (alumina).

Parameter	Symbol	Units	Value
Density	ρ_d	kg m^{-3}	3970
Elastic compliance	s_d	m^2 N^{-1}	2.5×10^{-12}

Table 4. Properties of piezoelectric material (PC5 Type II).

Parameter	Symbol	Units	Value
Density	ρ_p	kg m^{-3}	7750
Elastic compliance (short)	s^E	m^2 N^{-1}	17.2×10^{-12}
Elastic compliance (open)	s^D	m^2 N^{-1}	9.4×10^{-12}
Charge constant	d_p	C N^{-1}	409×10^{-12}
Permittivity	ϵ^T	Fa m^{-1}	1.5×10^{-8}

where s_d is the elastic compliance of the dielectric material and S_d is the dielectric strain. The properties of the dielectric material used in the numerical model can be found in table 3.

3.3. Piezoelectric model

The longitudinal displacement waves induced by the magnetostrictive emitter are transmitted through the whole structure, producing an induced electric charge in the poles of the piezoelectric receiver. This charge is directly related to the piezoelectric strain transmitted by the dynamic behaviour of the structure on the piezoelectric stack. When the current measurement transformer is subjected to time-dependent external excitation, the piezoelectric strain shows a time evolution which is described by the structural dynamic interaction among magnetostrictive, dielectric and piezoelectric parts. Thus, the variation of strain with respect to time produces an electric charge variation which eventually leads to the establishment of an electric current.

Linear piezoelectric constitutive behaviour is used to compute the receiver response. The model corresponds to the classical piezoelectric model reported elsewhere; see for instance [20]. Therefore, the constitutive equations are

$$\begin{aligned} S_\mathrm{p} &= s^\mathrm{E} T_\mathrm{p} + d_\mathrm{p} E_\mathrm{p} \\ D_\mathrm{p} &= d_\mathrm{p} T_\mathrm{p} + \epsilon^\mathrm{T} E_\mathrm{p} \end{aligned} \tag{2}$$

where S_p is the piezoelectric strain, s^E the elastic compliance at constant electric field, d_p is the piezoelectric constant, E_p the piezoelectric electric field, D_p the electric displacement and ϵ^T the permittivity at constant stress. In table 4 the piezoelectric material properties are shown.

Once the induced piezoelectric strain is computed by means of the finite element model the corresponding output can be obtained depending on the electronic circuit used to measure the output. Two configurations have been tested: open and short circuit layouts.

Open circuit layout implies that there is no induced electric charge, that is, $D_\mathrm{p} = 0$. Using equations (2) and assuming uniform electrical field, the relationship between the piezoelectric strain and the piezoelectric open circuit voltage, V_oc, is

$$V_\mathrm{oc} = -\frac{d_\mathrm{p} B}{\epsilon^\mathrm{T} s^\mathrm{D}} S_\mathrm{p}$$

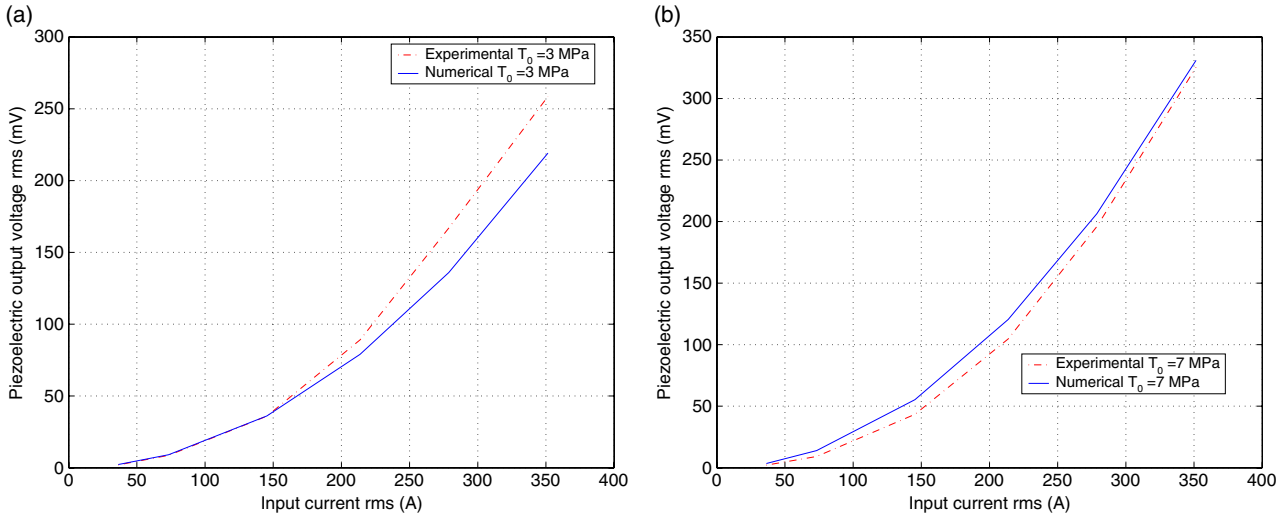

Figure 5. Open circuit voltage function of current input for precompression of (a) $T_0 = 3$ MPa and (b) $T_0 = 7$ MPa.

where B is the thickness of the piezoelectric stack, and $s^{\mathrm{D}} = s^{\mathrm{E}} - d_{\mathrm{p}}^2/\epsilon^{\mathrm{T}}$ is the elastic compliance at constant electric displacement.

The piezoelectric short circuit current is computed taking into account that the piezoelectric voltage or electric field is zero, that is, $E_{\mathrm{p}} = 0$, and taking into account equations (2) the corresponding relationship between piezoelectric strain and short circuit current, I_{sc}, is

$$I_{\mathrm{sc}} = A\frac{\mathrm{d}D_{\mathrm{p}}}{\mathrm{d}t} = \frac{\mathrm{d}_{\mathrm{p}}A}{s^{\mathrm{E}}}\frac{\mathrm{d}S_{\mathrm{p}}}{\mathrm{d}t}$$

where A is the piezoelectric stack cross section.

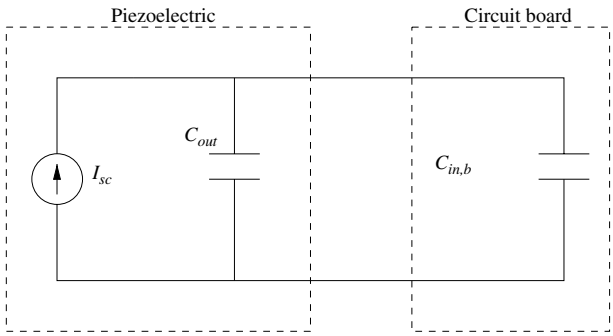

Figure 6. Equivalent electronic circuit scheme of the short circuit test.

3.4. Finite element model

The aforementioned constitutive equations, together with axial linear momentum balance, equation (1) and small displacement definition of strain, that is $S = \partial u/\partial x$, establish the system of partial differential equations to be solved. The finite element method has been chosen to numerically obtain the current sensor performance and structural response. Taking into account continuity between displacement and stress fields, the contribution of the auxiliary mechanical structure, and applying an standard finite element discretization to (1), the following set of ordinary differential equations is obtained:

$$\boldsymbol{M}\cdot\boldsymbol{a} + \boldsymbol{C}\cdot\boldsymbol{v} + \boldsymbol{K}\cdot\boldsymbol{u} = \boldsymbol{F} \tag{3}$$

where $\boldsymbol{M}$, $\boldsymbol{C}$, and $\boldsymbol{K}$ stand for the mass, damping and stiffness matrices respectively, and $\boldsymbol{a}$, $\boldsymbol{v}$, $\boldsymbol{u}$, and $\boldsymbol{F}$ are the acceleration, velocity, displacement and nodal force vectors, respectively.

Dissipation has been taken into account using a proportional damping, more commonly known as Rayleigh damping. Using this scheme, the damping matrix is computed as a linear combination of the stiffness and mass matrices:

$$\boldsymbol{C} = \alpha\boldsymbol{M} + \beta\boldsymbol{K} \tag{4}$$

where α and β stand for the mass and stiffness proportional damping constants, respectively. Once the assembly process has been performed the mass and stiffness matrices are obtained and therefore the damping matrix can be easily computed.

To obtain the time response to the alternating magnetic field acting upon the current sensor, a standard finite difference time discretization has been used to solve the system of ordinary differential equations (3). More precisely, a Newmark scheme has been implemented following the algorithmic consideration mentioned elsewhere; see for instance [9]. In particular, a trapezoidal rule has been chosen because of unconditional stability, implicit and second order of accuracy properties.

4. Comparison between numerical and experimental results

The comparison between computer simulation results and experimental data of the current sensor are presented in this section. During the experimental program of the current sensor two main sorts of test have been considered: that is, the input/output ratio for open circuit and short circuit configurations.

The proportional damping method used in the model, equation (4), depends on two parameters, α and β, and it

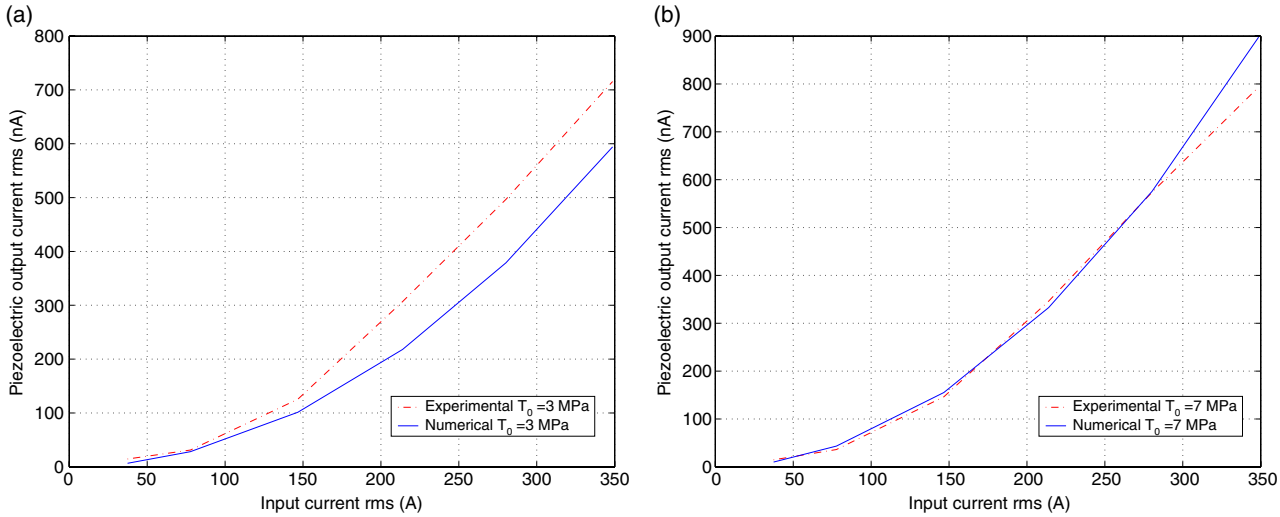

Figure 7. Short circuit current function of current input for precompression of (a) $T_0 = 3$ MPa and (b) $T_0 = 7$ MPa.

is common practice that they must be determined from the damping ratio of the structure. The damping ratio has been obtained by means of the fitting of numerical response and experimental results. After the comparison of both numerical and experimental data a value of damping ratio of 20% at 50 Hz has been obtained to fit the experimental data accurately enough to numerical simulations. Once the determination of damping ratio has been carried out, it can be said that the simple model proposed obtains accurate results not only for one sort of electronic tests but for all the tests considered.

In figure 4 the equivalent circuit scheme of the open circuit to measure the output circuit voltage is shown. The piezoelectric signal is analysed by an oscilloscope. From the electronic point of view, the piezoelectric receiver can be regarded as a voltage source, V_{oc}, associated with a capacitor of capacity C_{out} determined by the permittivity properties of the piezoelectric material. Additionally, the oscilloscope presents an input impedance formed by a resistance $R_{in,o}$, associated in parallel with a capacitor, $C_{in,o}$. Despite the fact that formally there is some resistance between the piezoelectric and the oscilloscope, this resistance is not considered because is negligible when it is compared to the other impedances. This consideration is also used for the short circuit configuration.

The input current is a current signal at 50 Hz frequency. The tests are performed at different primary current root mean square levels which range between 50 and 350 A. The output signal of the current sensor, the root mean square of the open circuit voltage, is measured and computed at every input level. In figure 5 the output voltage, that is the piezoelectric voltage, a function of the input current, namely the primary current, is shown at two precompression levels of 3 and 7 MPa for both experimental and numerical results at a primary frequency of 50 Hz.

Figure 6 presents the equivalent circuit scheme of the short circuit to measure the output circuit current. The piezoelectric signal is analysed using a circuit board with an impedance of capacity, $C_{in,b}$. A more detailed model of the circuit board could include a resistor in parallel. However, this resistor presents a very high impedance when it is compared to the capacitor impedance at frequencies of 50 Hz; thus, the resistor can be neglected. In this case the piezoelectric receiver can be considered as a current source, I_{sc}, and the same capacitor of the short circuit, C_{out}. The tests are performed at the same primary current levels of the open circuit test. The root mean square of the short circuit current is measured and computed at every input level. In figure 7 the piezoelectric output current function of the input current is shown at two precompression levels of 3 and 7 MPa for both experimental and numerical results at a primary frequency of 50 Hz.

Both experimental and numerical data show that a high precompression value implies a high output signal, for either open or short circuit layouts. This trend is a direct outcome of the well known magnetostrictive behaviour under compression which is certainly quite well modelled, and it can be verified by the experimental data.

5. Conclusions

The main conclusion that can be drawn from the experimental tests and design is that a magnetostrictive emitter coupled to a piezoelectric receiver through a dielectric material can be used to measure current in high-voltage lines. Both experimental and numerical modelling data have shown that a measurable current can be obtained to determine the actual current of the high-voltage line. The current sensor development is currently in the manufacturing process of the actual sensor to be tested in real power transmission lines.

The output signal dependence upon input current is quite well modelled in this paper and shows that despite its simplicity, the numerical model can be regarded as an accurate enough tool to evaluate preliminary designs. It is evident that the numerical modelling can be improved by means of the incorporation of more sophisticated constitutive models, especially those referring to the magnetostrictive emitter which take into account the hysteretic behaviour. However, it should be remarked that one of the modelling program requirements was the development of computational low-cost models. Therefore, taking into account accuracy and computational

cost, a trade-off between them needed to be achieved. At the design stage the main concern was the development of a numerical model able to aid the manufacturing process by obtaining accurate enough data about the performance of the sensor. In this regard the constitutive models used satisfy the initial requirements of accuracy and computational cost.

Currently the authors are working on the development of a new phenomenologically based constitutive model for the magnetostrictive material that will be able to improve the numerical model by means of a better description of the hysteretic behaviour and the energy dissipated by the sensor in the dynamic process.

Acknowledgments

This work is currently supported by the European Commission through the IELAS project (contract number G5RD-CT-2001-0054) under the Competitive and Sustainable Growth Research Programme. This support is gratefully acknowledged. The results shown here have been possible through the coordinated effort of a group of institutions and persons. The authors would like to acknowledge and thank C Martinez, C Hita and E Barroso from REE, P Albertelli and P Ferrari from Ansaldo Ricerche, T Prescott from Enterprise Ireland, N Jones from Morgan Matroc, V Ruch from Techsonic, C Schmaus from Siegert, and M J Martin from UPCO.

References

[1] Bohnert K, Gabus P, Nehring J and Brandle H 2002 Temperature and vibration insensitive fiber-optic current sensor *J. Lightwave Technol.* **20** 267–76

[2] Butler J L, Butler A L and Butler S C 1993 Hybrid magnetostrictive piezoelectric Tonpilz transducer *J. Acoust. Soc. Am.* **94** 636–41

[3] Calkins F T, Smith R C and Flatau A B 2000 Energy-based hysteresis model for magnetostrictive transducers *IEEE Trans. Magn.* **36** 429–39

[4] Carman G P and Mitrovic M 1995 Nonlinear constitutive relations for magnetostrictive materials with applications to 1-d problems *J. Intell. Mater. Syst. Struct.* **6** 673–83

[5] Dapino M J, Smith R C, Calkins F T and Flatau A B 2002 A coupled magnetomechanical model for magnetostrictive transducers and its application to Villari-effect sensors *J. Intell. Mater. Syst. Struct.* **13** 737–47

[6] Dapino M J, Smith R C and Flatau A B 2000 Structural magnetic strain model for magnetostrictive transducers *IEEE Trans. Magn.* **36** 545–56

[7] Dong S X, Li J F, Viehland D, Cheng J and Cross L E 2004 A strong magnetoelectric voltage gain effect in magnetostrictive–piezoelectric composite *Appl. Phys. Lett.* **85** 3534–6

[8] Hotate K and Konishi Y 2002 Formulas describing error induced by fiber linear-birefringence in fiber-optic current sensors *15th Optical Fiber Sensors Conf. Technical Digest (Portland, Oregon, USA, May 2002)* vol 1, pp 557–60

[9] Hughes T J R 1987 *The Finite Element Method* (Englewood Cliffs, NJ: Prentice-Hall)

[10] Jiles D C 1995 Theory of the magnetomechanical effect *J. Phys. D: Appl. Phys.* **28** 1537–46

[11] Jiles D C and Atherton D L 1984 Theory of the magnetisation process in ferromagnets and its application to the magnetomechanical effect *J. Phys. D: Appl. Phys.* **17** 1265–81

[12] Jiles D C 1986 Theory of ferromagnetical hysteresis *J. Magn. Magn. Mater.* **61** 48–60

[13] Lee B 2003 Review of the present status of optical sensors *Opt. Fiber Technol.: Mater. Dev. Syst.* **9** 57–79

[14] Lin W-W 2003 Fiber-optic current sensor *Opt. Eng.* **42** 896–7

[15] Park G, Muntges D E and Inman D J 2003 Self-repairing joints employing shape-memory alloy actuators *JOM-J. Miner. Met. Mater. Soc.* **55** 33–7

[16] Perez-Millán P, Martínez-León L, Diez A, Cruz J L and Andres M V 2002 A fiber-optic current sensor with frequency-codified output for high-voltage systems *IEEE Photon. Technol. Lett.* **8** 1339–41

[17] Prieto J L, Aroca C, López E, Sánchez M C and Sánchez P 2000 Magnetostrictive-piezoelectric magnetic sensor with current excitation *J. Magn. Magn. Mater.* **215** 756–8

[18] Sablik M J and Giles D C 1993 Coupled magnetoelastic theory of magnetic and magnetostrictive hysteresis *IEEE Trans. Magn.* **29** 2113–23

[19] Sanders B, Cowan D and Scherer L 2004 Aerodynamic performance of the smart wing control effectors *J. Intell. Mater. Syst. Struct.* **15** 293–303

[20] Srinivasan A V and McFarland D M 2001 *Smart Structures. Analysis and Design* (Cambridge: Cambridge University Press)